Chapter 6

Microcanonical properties

6.1 Microcanonical definitions

Consider a system of N classical particles on a disk of radius R whose interaction is described by a Plummer softened potential [PLU11, YEP97]

$$\varphi_{ij} = -\frac{Gm_i m_j}{\sqrt{s^2 + (\mathbf{q}_i - \mathbf{q}_j)^2}}, \tag{6.1}$$

where m_i and $\mathbf{q}_i = \{q_i^1, q_i^2\}$ are the mass and position of particle i respectively, s is the softening length and G is the gravitational constant. The fixed total energy E is described by the Hamiltonian

$$\mathcal{H} = \sum_i \frac{\mathbf{p}_i^2}{2m_i} + \varphi(\mathbf{q}), \tag{6.2}$$

where $\mathbf{p}_i = \{p_i^1, p_i^2\}$ is the linear momentum of particle i, $\varphi = \sum_{i<j} \varphi_{ij}$. $\mathbf{q}$ is a $2N$–dimensional vector whose coordinates are $\{\mathbf{q}_1, \ldots, \mathbf{q}_N\}$, representing the spatial configuration. $\mathbf{q}$ is an element of the spatial configuration space V_c, $\mathbf{q} \in V_c \subset \mathbb{R}^{2N}$.

The entropy S is given through Boltzmann's principle

$$S(E, L, N) \doteq \ln W(E, L, N), \tag{6.3}$$

where $W(E, L, N)$ is the volume of the accessible phase–space at E, L and N fixed (under the assumptions given in chap. 5 on page 87)

$$\begin{aligned} W\big(E, L, N\big) &= \frac{1}{N!} \int \prod_{i=1}^{N} \left(\frac{d\mathbf{p}_i d\mathbf{q}_i}{(2\pi\hbar)^2} \right) \delta\big(E - \mathcal{H}\big) \delta^{(2)}\big(\sum_i \mathbf{p}_i\big) \\ &\quad \times \delta\big(L - \sum_i \mathbf{q}_i \times \mathbf{p}_i\big) \delta^{(2)}\big(\sum_i \mathbf{q}_i\big), \end{aligned} \tag{6.4}$$

where $\mathbf{q}_i \times \mathbf{p}_i = q_i^1 p_i^2 - q_i^2 p_i^1$. After integration over the momenta eq. (6.4) becomes [LAL99, CL98]

$$W\big(E, L, N\big) = \mathcal{C} \int_{V_c} d\mathbf{q}\, \frac{1}{\sqrt{I}} E_r^{N-5/2} \delta^{(2)}\big(\sum_i \mathbf{q}_i\big), \tag{6.5}$$

where $\mathcal{C} = \frac{(2\pi)^{(N-9/2)} \prod_i m_i}{(2\pi\hbar)^{2N} N! (\sum_i m_i) \Gamma(N-3/2)}$ is a constant, $I = \sum_i m_i \mathbf{q}_i^2$ is the inertial momentum and $E_r = E - \frac{L^2}{2I} - \varphi$ the remaining energy [a]. From the point of view of the remaining energy, if $L \neq 0$ one can already notice that the equilibrium properties are the result of a competition between two terms: the rotational energy $\frac{L^2}{2I}$ and the potential energy φ. The former tries to drive the particles away from the center of mass in order to increase I whereas the latter tries to group the particles together in order to decrease φ, but since the center of mass is fixed this will lead to a concentration of particles near the center and consequently will decrease I.

The microcanonical temperature T is defined by

$$\frac{1}{T} \doteq \beta \doteq \frac{\partial S}{\partial E} = \langle \frac{N - 5/2}{E_r} \rangle, \tag{6.6}$$

where $\langle \cdot \rangle$ is the microcanonical average

$$\langle \mathcal{O} \rangle = \frac{\mathcal{C}}{W} \int_{V_c} d\mathbf{q} \frac{\mathcal{O}(\mathbf{q})}{\sqrt{I}} E_r^{N-5/2} \delta^{(2)}\big(\sum_i \mathbf{q}_i\big). \tag{6.7}$$

The angular velocity ω is defined as minus the conjugate force of L times T [DGLR89]

$$\omega \doteq -\frac{1}{\beta} \frac{\partial S}{\partial L} = \frac{\langle \frac{L}{I} E_r^{-1} \rangle}{\langle E_r^{-1} \rangle}. \tag{6.8}$$

$\gamma\beta$ is defined has the conjugate of L^2

$$\gamma\beta \doteq \frac{\partial S}{\partial L^2} = -\langle \frac{1}{2I} \frac{N - 5/2}{E_r} \rangle, \tag{6.9}$$

$$\omega = -2L\gamma. \tag{6.10}$$

6.2 Momentum average and dispersion

In this section the average and the dispersion of the linear momentum of a particle is derived, its mean angular velocity is also computed and related to the one of the system as defined in eq. (6.8).

The derivation of $\langle \mathbf{p}_k \rangle_{\mathbf{q}_k}$ the average momentum of particle k at fixed position $\mathbf{q}_k$ (while the other particles are free) is similar to that of W. Details of the derivation can be found in Appendix C on page 133, and the result is

$$\langle \mathbf{p}_k \rangle_{\mathbf{q}_k} = L \langle I^{-1} \rangle_{\mathbf{q}_k} m_k \sum_{\alpha,\gamma=1}^{2} \epsilon_{\alpha\gamma} q_k^\gamma \hat{\mathbf{e}}_\alpha, \tag{6.11}$$

where ϵ is the antisymmetric tensor of rank 2 and $\hat{\mathbf{e}}_\alpha$ the unit vector of coordinate α. Equation (6.11) shows that $\langle \mathbf{p}_k \rangle_{\mathbf{q}_k}$ is a vector perpendicular to $\mathbf{q}_k$ whose module is a function of $\|\mathbf{q}_k\|$. In other words the orbit of a particle is in the mean circular (this result is expected since the system is rotationally symmetric). One can compute $\langle \omega_k \rangle_{\mathbf{q}_k}$ the

[a] the number $\frac{5}{2}$ in eq. (6.5) is due to the different delta functions in eq. (6.4) that are integrated out: $\frac{1}{2}$ for the conservation of L, $2 \cdot \frac{1}{2} = 1$ for $\mathbf{P}$ and one for the total energy E.

mean angular velocity of k at distance $\|\mathbf{q}_k\|$ by first considering $\langle L_k \rangle_{\mathbf{q}_k}$ the mean angular momentum of k at distance $\|\mathbf{q}_k\|$

$$\begin{aligned} \langle L_k \rangle_{\mathbf{q}_k} &\doteq \mathbf{q}_k \times \langle \mathbf{p}_k \rangle_{\mathbf{q}_k} \\ &= L \langle I^{-1} \rangle_{\mathbf{q}_k} I_k, \end{aligned} \tag{6.12}$$

where $I_k = m_k \mathbf{q}_k^2$. The angular mean velocity of a particle on a circular orbit is classically linked to $\langle L_k \rangle_{\mathbf{q}_k}$ by

$$\langle L_k \rangle_{\mathbf{q}_k} = \langle \omega_k \rangle_{\mathbf{q}_k} I_k. \tag{6.13}$$

Using eqs. (6.12) and (6.13) leads to the following expression for $\langle \omega_k \rangle_{\mathbf{q}_k}$

$$\langle \omega_k \rangle_{\mathbf{q}_k} = L \langle I^{-1} \rangle_{\mathbf{q}_k}. \tag{6.14}$$

The dependence of $\langle \omega \rangle_{\mathbf{q}_k}$ on $||\mathbf{q}_k||$ is of the order $1/N$ [b], therefore for large N, $\langle \omega \rangle_{\mathbf{q}_k}$ becomes (see eq. (6.8) on the preceding page)

$$\langle \omega_k \rangle_{\mathbf{q}_k} \sim L \langle I^{-1} \rangle \approx \langle \omega \rangle. \tag{6.15}$$

For large N the mean angular velocity is the same for all the particles at any distance from the center, in other words the system in the mean rotates like a solid body. Moreover $\langle \omega_k \rangle_{\mathbf{q}_k}$ corresponds to the thermostatistical angular velocity ω defined by eq. (6.8) on the facing page. These are also a classical results for extensive systems at low L [DGLR89, LL94]. Note also that these results do not depend explicitely on the interaction potential φ.

The momentum dispersion $\sigma_{\mathbf{p}_k}$ can also be derived. Using eq. (6.11) and eq. (C.16) on page 135, one gets for large N

$$\begin{aligned} \sigma_{\mathbf{p}_k}^2 &\equiv \langle \mathbf{p}_k^2 \rangle_{\mathbf{q}_k} - \langle \mathbf{p}_k \rangle_{\mathbf{q}_k}^2 \\ &\sim 2\frac{m_k}{\beta} + I_k L^2 m_k \left(\langle I^{-2} \rangle - \langle I^{-1} \rangle^2 \right) \end{aligned} \tag{6.16}$$

The second term of eq. (6.16) is proportional to the square of the dispersion of I^{-1} and to $\mathbf{q}_k^2$ ($I_k = m_k \mathbf{q}_k^2$). When this term vanishes relatively to the first one, e.g. when the fluctuations of I^{-1} are small, or at high energy (low β) and low L, the usual dispersion of the Maxwell–Boltzmann distribution is recovered. This term also gives a correction to the usual equipartition theorem; for large N

$$\begin{aligned} \langle E_k \rangle &\equiv \frac{\sigma_{\mathbf{p}_k}^2}{2m_k} \\ &\sim T + \frac{I_k L^2}{2} \left(\langle I^{-2} \rangle - \langle I^{-1} \rangle^2 \right), \end{aligned} \tag{6.17}$$

where $\langle E_k \rangle$ is the average internal kinetic energy (without the contribution from the collective hydrodynamic rotational movement) of particle k. Again this correction is position–dependent via I_k. In the regimes where the fluctuations of the mass distribution cannot be neglected in eqs. (6.16) and (6.17) (e.g. at phase transitions) an estimate of the temperature based on the velocity dispersion would suggest that the temperature is smaller in the core than at the edge. At high energies and in the limit $N \to \infty$ the fluctuations of I^{-1} should vanish faster than L ($\sim N$) grows in order to recover the equipartition of energy. However this scaling behavior is not known in the whole parameter space. These fluctuations might play a non–trivial role in phase transition regions even for large N.

[b] $\langle I^{-1} \rangle_{\mathbf{q}_k} = \langle I^{-1} \rangle + \mathcal{O}(N^{-1})$

6.3 Numerical method

From now all the particles have the same mass, i.e. $m_i = m$, $\forall i = 1, \cdots, N$ and the following dimensionless variables are used

$$E \rightarrow \epsilon = \frac{ER}{Gm^2N^2}, \tag{6.18a}$$

$$L \rightarrow l^2 = \Omega = \frac{L^2}{2Gm^3RN^2}, \tag{6.18b}$$

$$s \rightarrow \sigma = \frac{s}{R}, \tag{6.18c}$$

$$\mathbf{q} \rightarrow \mathbf{r} = \frac{\mathbf{q}}{R}, \tag{6.18d}$$

$$V_c \rightarrow v_c, \tag{6.18e}$$

$$\varphi \rightarrow \phi = \frac{R}{Gm^2N^2}\varphi = -\frac{1}{N^2}\sum_{i<j}\frac{1}{\sqrt{\sigma^2 + (\mathbf{r}_i - \mathbf{r}_j)^2}}, \tag{6.18f}$$

$$I \rightarrow I = \sum_i r_i^2. \tag{6.18g}$$

The weight is now

$$W(\epsilon, \Omega) = \mathcal{C}' \int_{v_c} d\mathbf{r} \frac{1}{\sqrt{I}} \epsilon_r^{N-5/2} \delta^{(2)}\big(\sum_i \mathbf{r}_i\big), \tag{6.19}$$

where $\epsilon_r = \epsilon - \frac{\Omega}{I} - \phi$ is the dimensionless remaining energy and $\mathcal{C}'$ a constant. Later on this constant is omitted since it plays classically no significant role (it only shifts the entropy by $\log \mathcal{C}'$). The derivatives of entropy (β, ω, ...) are now dimensionless quantities.

One usually estimates (6.19) by means of some Monte Carlo algorithm, updating the positions $\mathbf{r}$ by some small amount $\delta\mathbf{r}$ in order to get a good pass acceptance and using the configuration weight $W(\mathbf{r}) \doteq \frac{1}{\sqrt{I}}\epsilon_r^{N-5/2}$ in the Metropolis pass. Unfortunately this strategy does not really work (within a reasonable CPU–time), because the $2N$–dim configuration weight–landscape at fixed ϵ and Ω presents troughs and high peaks [TA99], so exploring the total configuration–space (or at least a subset containing the highest peaks) would take a very long, in practice infinite, time. This weight–landscape looks like the energy–landscape found in spin–glass systems [MPRTZ00].

The strategy adopted here is partly described in the following. First eq. (6.19) can be rewritten as

$$W(\epsilon, \Omega) = \int dI\, d\phi\, Bg(I, \phi)\, \frac{1}{\sqrt{I}} \epsilon_r^{N-5/2}, \tag{6.20}$$

where

$$Bg(I, \phi) = \int_{v_c} d\mathbf{r} \delta\left(I'(\mathbf{r}) - I\right) \delta\left(\phi'(\mathbf{r}) - \phi\right) \big(\sum_i \mathbf{r}_i\big). \tag{6.21}$$

$Bg(I, \phi)$ is the density of spatial configurations at given I and ϕ. Given Bg one can compute W, S and its derivatives for *any* ϵ and Ω, e.g.

$$\begin{aligned} \gamma &= \frac{1}{\beta}\frac{\partial S}{\partial \Omega} \\ &= -\frac{N - 5/2}{\beta} \frac{\int dI\, d\phi\, Bg(I, \phi)\, I^{-3/2} \epsilon_r^{N-7/2}}{W(\epsilon, \Omega)}. \end{aligned} \tag{6.22}$$

The expectation value $\langle \mathcal{O} \rangle$ of an observable $\mathcal{O}(\mathbf{r})$ can be estimated if Bg and $\langle \mathcal{O} \rangle_{I,\phi}$ are known

$$\begin{aligned} \langle \mathcal{O} \rangle &\equiv \frac{\int_{v_c} d\mathbf{r}\, \mathcal{O}(\mathbf{r}) I^{-1/2} \epsilon_r^{N-5/2} \delta^{(2)}\left(\sum_i \mathbf{r}_i\right)}{\int_{v_c} d\mathbf{r}\, I^{-1/2} \epsilon_r^{N-5/2} \delta^{(2)}\left(\sum_i \mathbf{r}_i\right)} \\ &= \frac{\int dI\, d\phi\ \langle \mathcal{O} \rangle_{I,\phi} Bg\,(I,\phi)\, I^{-1/2} \epsilon_r^{N-5/2}}{W\,(\epsilon,\Omega)}, \end{aligned} \tag{6.23}$$

where

$$\langle \mathcal{O} \rangle_{I,\phi} = \frac{\int_v d\mathbf{r}\, \mathcal{O}(\mathbf{r}) \delta\,(I'-I)\,\delta\,(\phi'-\phi)\,\delta^{(2)}\left(\sum_i \mathbf{r}_i\right)}{Bg\,(I,\phi)}. \tag{6.24}$$

Now, the task is to compute $Bg(I,\phi)$ and $\langle \mathcal{O} \rangle_{I,\phi}$. *A priori* $Bg(I,\phi)$ is highly peaked around the values of I and ϕ that describe the gas (disordered) phase and should drop rapidly down to the edges. Nevertheless a good estimate of $Bg(I,\phi)$ is needed for almost all values taken by (I,ϕ) even when $Bg(I,\phi)$ is very small comparing to its maximum. For example at small total energy ϵ only the part of $Bg(I,\phi)$ for which $\epsilon_r = \epsilon - \frac{\Omega^2}{I} - \phi > 0$ contributes to the integral (6.20) on the preceding page.

In order to get a good estimate of Bg an iterative scheme inspired by multicanonical algorithms has been used [LEE93, BH93, FS89, SMI96]. For further details see app. B.3.

In the present thesis results for $\sigma = 0.05$ and $N = 20$ are presented [c]. No qualitative changes are expected with larger number of particles (preliminary studies for N up to 100 support all the following results).

6.4 Results

6.4.1 Entropy and its derivatives

Figure 6.1 on the following page shows the entropy surface S as a function of ϵ and Ω. The ground state energy $\epsilon_g(\Omega)$ (thick line in Fig. 6.1) increases with Ω;. ϵ_g classically corresponds to $\epsilon_r = 0$ implying $S = -\infty$. For all Ω, $\epsilon_g(\Omega)$ is a concave function of Ω, i.e. $\frac{\partial^2 \epsilon_g}{\partial \Omega^2} \leq 0$; at high Ω ($\Omega \gtrsim 12$) it is almost linear $\frac{\partial^2 \epsilon_g}{\partial \Omega^2} \to 0^-$. In sec. 6.4.4 dramatic consequences for the canonical ensemble introduced by Klinko and Miller [KM00] resulting from this quasi–linear behavior are discussed.

At fixed Ω, $S(\epsilon)$ is not concave for all ϵ but shows for some energy interval a convex intruder which signals a first order phase transition with negative specific heat capacity $\left(\frac{\partial \beta}{\partial \epsilon} > 0\right)$. This can be better viewed by plotting $\beta(\epsilon,\Omega) = \frac{\partial S}{\partial \epsilon}$ (Fig. 6.2 on page 95). Here the counter part of the entropy–intruder is a region of multiple valued $\epsilon(\beta)$. This is the case for β between 15 and 20.

The latent heat at fixed Ω, $q_\epsilon(\Omega)$ decreases for $0 \leq \Omega \lesssim 12$ and is a constant for $\Omega > 12$. There is no critical value of Ω, Ω_c above which $S(\epsilon)$ is concave for all ϵ, i.e. there is a first order phase transition in the energy direction for all values of Ω. In another model for self–gravitating systems such a Ω_c was reported [LAL99], but not in the one presented in [KM00].

On Fig. 6.3 on page 96 the microcanonical angular velocity ω as a function of Ω and ϵ is plotted. As a direct consequence of eq. (6.8) on page 90, ω tends to zero with Ω, and at

[c] See in app. B.3 a discussion about the technical reasons that limit the value of N.

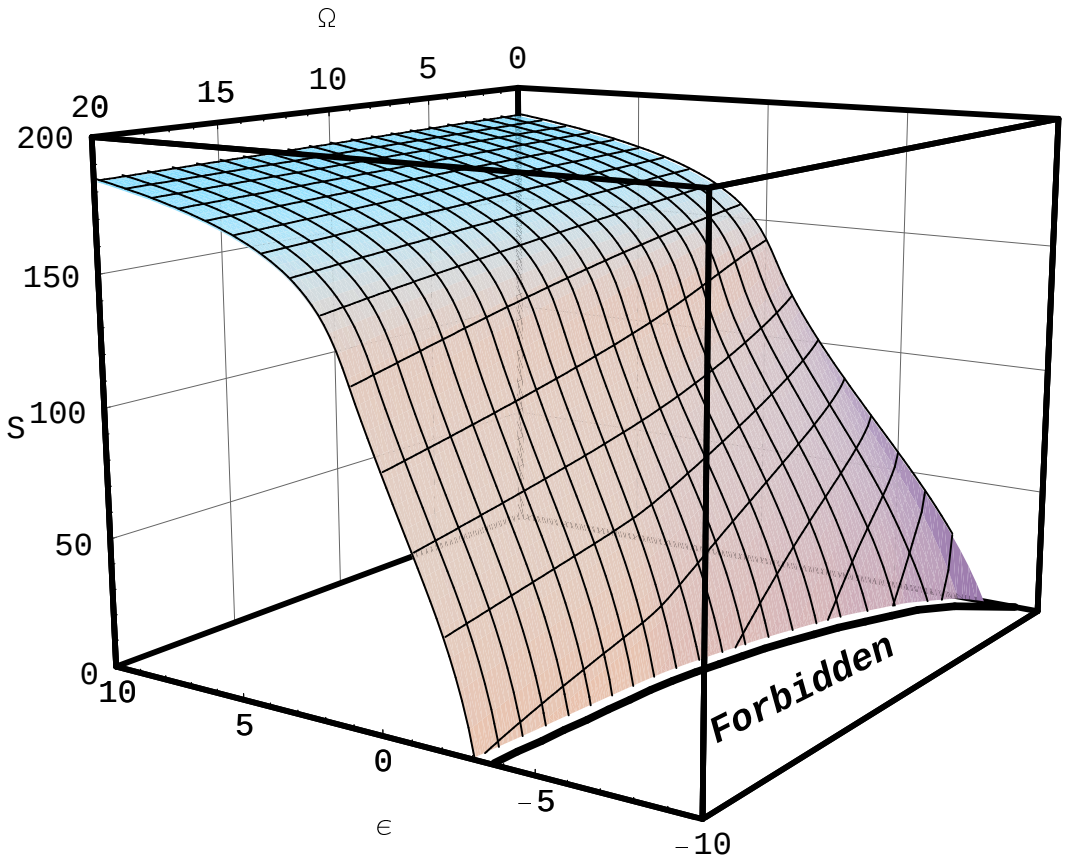

Figure 6.1: Entropy surface $S\left(\epsilon, \Omega = l^2\right)$, the mesh lines are at constant ϵ or constant Ω. The thick line is the projection of the $T = 0$ ($S \to -\infty$) isotherm. A convex intruder at constant Ω and for a certain energy range (e.g. $-2 < \epsilon < 0$ for $\Omega = 20$) can be seen for all Ω. S is not defined in the *forbidden* region; there the remaining energy ϵ_r is negative for any spatial configuration.

high energies ω is proportional to $\sqrt{\Omega} = l$ ($\propto L$). For low energies and $\Omega < 12$, ω exhibits some structures with peaks and troughs. In another words at fixed ϵ, ω is not necessarily an increasing function of Ω. At high Ω ($\Omega > 12$) and near the ground states ω is almost a constant. All these structures can be understood in terms of mass distributions which influence ω through I (see sec. 6.4.2).

6.4.2 Mass distribution

In order to understand the origin of the structures seen in the different microcanonical quantities (S, β, ω, ...) one has to have a closer look at the spatial configurations, i.e. at the mass distributions. One of the observable studied in this work is the mass density ρ (see eq. (6.23) and (6.24) on the preceding page). As the system is rotationally invariant, ρ can only be a function of r, the distance from the center of coordinates.

On Fig. 6.4 on page 97 ρ is plotted for different energies and for $\Omega = 0$ and $\Omega = 4$. For $\Omega = 0$ (Fig. 6.4(a)) the classical case (when E is the only fixed "extensive" parameter) is recovered. At high energy the system is in a homogeneous gas phase (flat ρ), when

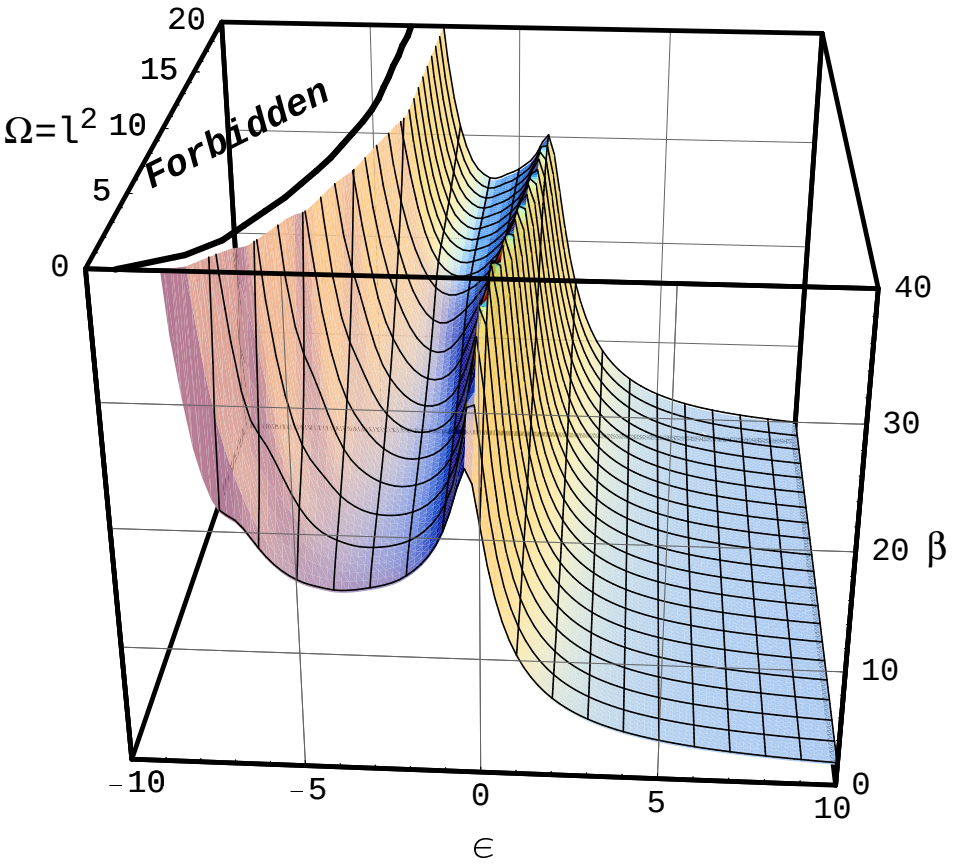

Figure 6.2: Inverse temperature $\beta(\epsilon, \Omega = l^2)$ surface. The mesh lines are at constant ϵ or constant Ω. The intruder in S at fixed Ω corresponds here to a multiple energy value for a given β and Ω, e.g. $\beta(\epsilon, \Omega = 0) = 20$ has three solutions $\epsilon_1 \approx 0$, $\epsilon_2 \approx -1$ and $\epsilon_3 \approx -6$. The thick line is the projection of the $\beta = \infty$ isotherm; β is not defined in the *forbidden* region.

the energy decreases the system undergoes a phase transition and eventually ends up in a collapse phase where a majority of particles are in a cluster near the center of coordinates (ρ peaked at $r = 0$). For $\Omega \neq 0$ (Fig. 6.4(b)) the situation is very different. At high energy the homogeneous gas phase is still present. But at low energy the system cannot collapse entirely at the center of mass. This is due to the rotational energy term ($\epsilon_{rot} = \frac{\Omega}{I}$) in the remaining energy, see eq. (6.19) on page 92. If the system contracts at the center then the inertial momentum I will tend to zero and therefore ϵ_{rot} will diverge leading to a negative remaining energy ϵ_r. So depending on the value of Ω the main cluster will eject a certain amount of particles in order to increase I. Near the ground state these "free" particles will eventually collapse to form a second cluster in order to decrease the potential energy ϕ. Due to the conservation of the center of mass, the position of the biggest cluster will be shifted from the center by a certain amount (see Fig. 6.4(b) at $\epsilon = -5$). At low Ω one particle will be ejected. With increasing Ω the number of ejected particles raises and this process stops when two equal–size clusters are formed. This explains the discreteness of the peaks in ω (Fig. 6.3 on the next page); the increase of the ground state energy $\epsilon_g(\Omega)$, because the potential energy of a single cluster of size N is smaller than the one of two

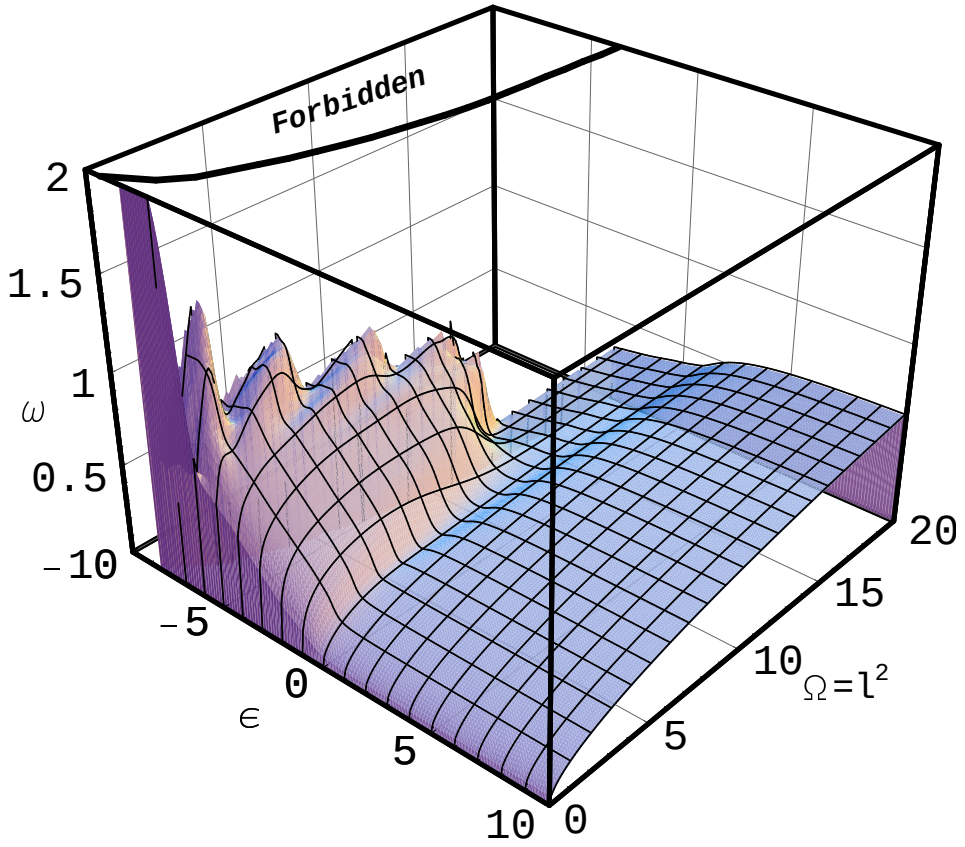

Figure 6.3: Microcanonical angular velocity $\omega\left(\epsilon, \Omega = l^2\right)$ surface. The mesh lines are at constant ϵ or constant Ω. ω is not defined in the *forbidden* region. At high energy $\omega \propto \sqrt{\Omega} = l$; Near the ground states ω shows a richer non–monotonic behavior with peaks and troughs for small Ω and has a nearly constant value for large Ω (see text).

well separated clusters. At high $\Omega \gtrsim 12$ the system undergoes a phase transition from a gas phase to a collapse phase with two equal size clusters close to the boundary. From one value of $\Omega = \Omega_1 > 12$ to another one $\Omega_2 > \Omega_1$ the whole entropy curve at fixed angular momentum is simply shifted along the energy axis, i.e. $S(\epsilon, \Omega_1) \approx S\left(\epsilon + \frac{\Omega_2 - \Omega_1}{N}, \Omega_2\right)$. So the ground state energy $\epsilon_g(\Omega)$ at high Ω is almost on a line of equation $\epsilon_g + \frac{\Omega}{N} + \phi_g \approx 0$, where $\frac{\Omega}{N}$ and ϕ_g are the rotational energy and the potential energy of 2 clusters of size $N/2$ at radius $r = 1$ respectively. This monotonic behavior has already be mentioned for all the thermodynamical variables e.g. S, β, ω, see Figs. 6.1 to 6.3 on pages 94–96.

One could object that, as ρ is only a function of r it cannot be used to infer the angular distribution of the particles, i.e. there is not enough information to say if a peak in ρ at $r_0 \neq 0$ corresponds to one or many clusters or to a uniform distribution of the particles lying on a circle of radius r_0 (ring). However at least at very low energy a many clusters (more than two) configuration is very unlikely and will not contribute to the average values for reasons linked to the configurational weight $W(\mathbf{r}) = \frac{1}{\sqrt{I}}\epsilon_r^{N-5/2}$. For simplicity let us assume that there is only one strong peak in ρ at $r = r_0 \neq 0$. Since the center of mass is fixed this cannot be the signature of a 1–cluster system. At least 2–clusters lying on a circle of radius r_0 are needed. All the n–clusters systems compatible with the assumed

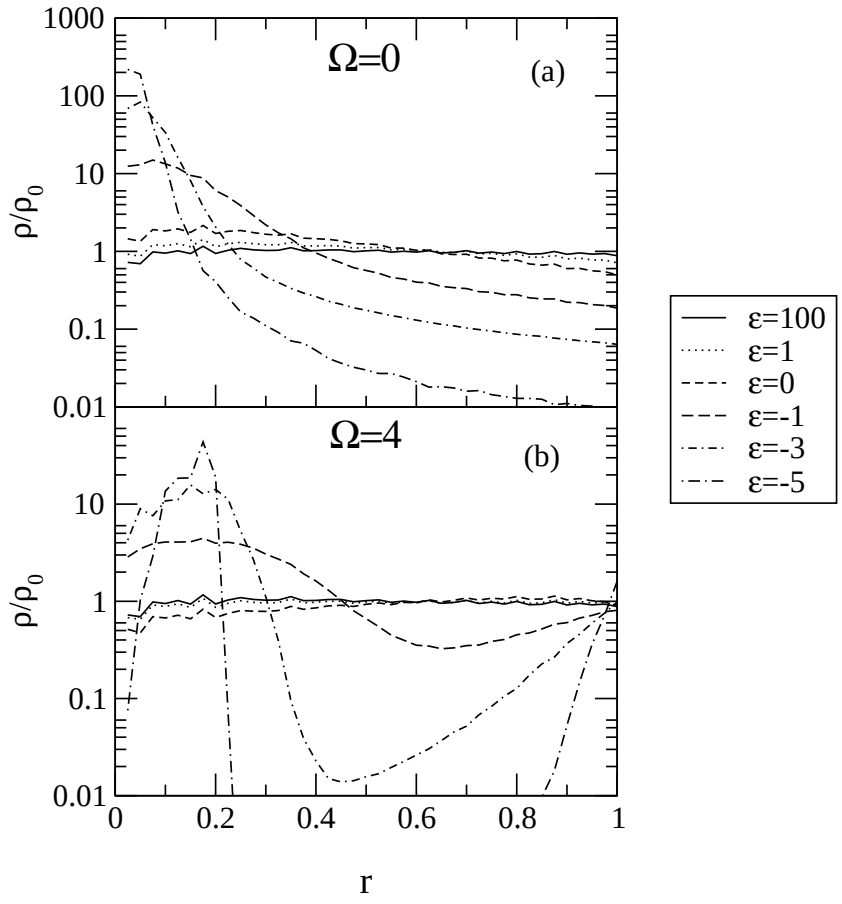

Figure 6.4: Density as a function of the distance from the center r for different values of energy ϵ and angular velocity Ω (arbitrary units). At high energy and for all Ω the density is flat; the system is in the homogeneous gas phase. Near the ground state the density shows one peak for $\Omega = 0$ (a) and two peaks for $\Omega > 0$ (b), which correspond respectively to a one cluster and to a two clusters phase surrounded by some gas (see text).

radial density have the same rotational energy $\frac{\Omega}{I} = \frac{\Omega}{Nr_0^2}$, but their corresponding potential energy ϕ_n are different. For example, with $\sigma = 0.05$, $r_0 = 0.5$ and $N = 24$ the ratio of potential energy is $\frac{\phi_2}{\phi_3} \simeq 1.7$. So at low energy, the remaining energy ϵ_r corresponding to a 2–clusters system will be much larger than the 3–clusters' one, leading to a *huge* difference [d] in the weight $W(\mathbf{r})$. So at low energy and for $\Omega \neq 0$ the 2–clusters case is dominant. At higher energies, the term $Bg(I, \phi)$ in eq. (6.19) on page 92 can compensate the difference in the weight $W(\mathbf{r})$ and allow many clusters configurations and eventually at high energy a complete random configuration on the ring of radius r_0 will dominate the average mass distribution.

This argument can be checked by studying other observables, for example the normalized distance distribution $P(d)$, i.e. the density of probability that the distance between two given particles is d. To probe the information given by $P(d)$, it has been estimated for four simple mass distributions: (a) 2–clusters, (b) 3–clusters, (c) ring, (d) uniform random

[d] The energy ϵ_r is put to a power of $\sim N$, see eq. (6.19).

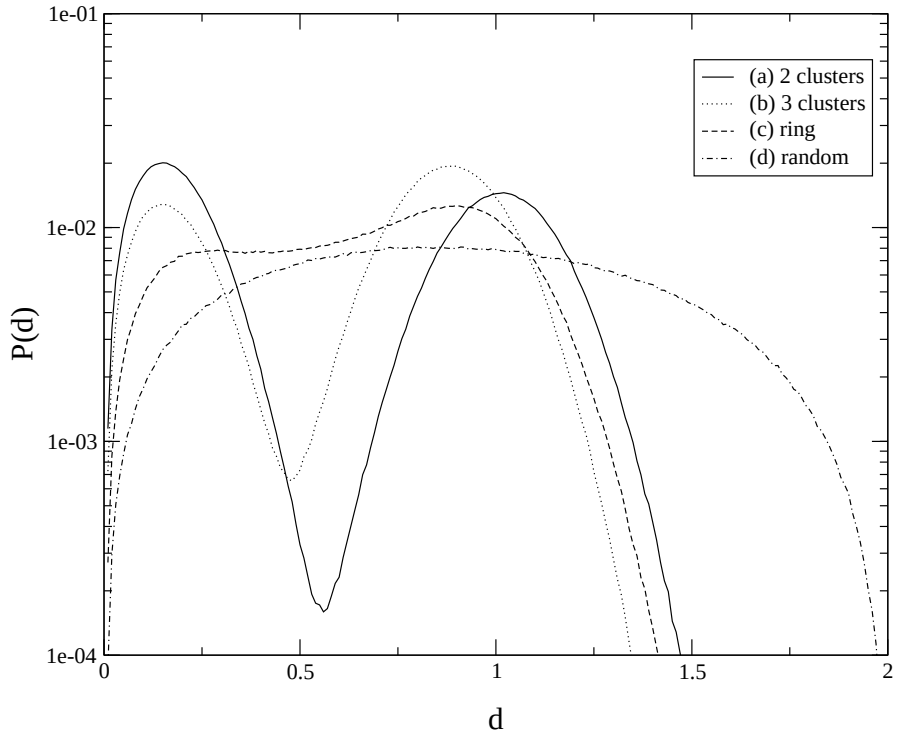

Figure 6.5: Average of $P(d)$ the distance distribution for different simulated spatial configurations. See text.

distribution. For (a), (b) and (c) the particles were put on a circle of radius $r_0 = 0.5$, and then randomly shifted several times (in order to give a spatial extension to these idealized initial configurations). Finally the $\frac{N(N-1)}{2}$ distances are recorded for all realizations and averaged. Figure 6.5 shows the average of $P(d)$ over 1000 realizations. Note that the density distribution $\rho(r)$ is by construction exactly the same for the three first cases, i.e. strongly peaked at r_0 with a width of about 0.5. The latter value depends on the shift one applies on the initial idealized spatial configurations.

As one can see on Fig. 6.5 that although the density distribution is the same for (a), (b) and (c), $P(d)$ gives some new insight on the mass distribution:

(a) There are two peaks, one at small d which corresponds to a clusterisation and another one at $r \simeq 1 = 2 \star r_0$; this is exactly the distance between the two clusters (more precisely between their center of mass). The areas under the small and large d peaks are equal. Indeed the number of short distance pairs is about $\frac{N^2}{4}$ which is also the number of pairs with $d \simeq 1$. The widths of the first and second peaks are (as expected) ~ 0.5 and $\sim 1 = 2 * 0.5$, respectively.

(b) There are again two peaks one at small d and another at $d \simeq 0.8 < 1$ and their respective widths are similar to the case (a). The large d is compatible with the length of one side of the equilateral triangle on top of which the idealized 3–clusters mass distribution has been built. This time the area under the large d peak is larger than the one under the short d peak, since the number of short distance pairs is about $\frac{N^2}{6}$ whereas the number of pairs with $d \simeq 0.8$ is $\frac{N^2}{3}$.

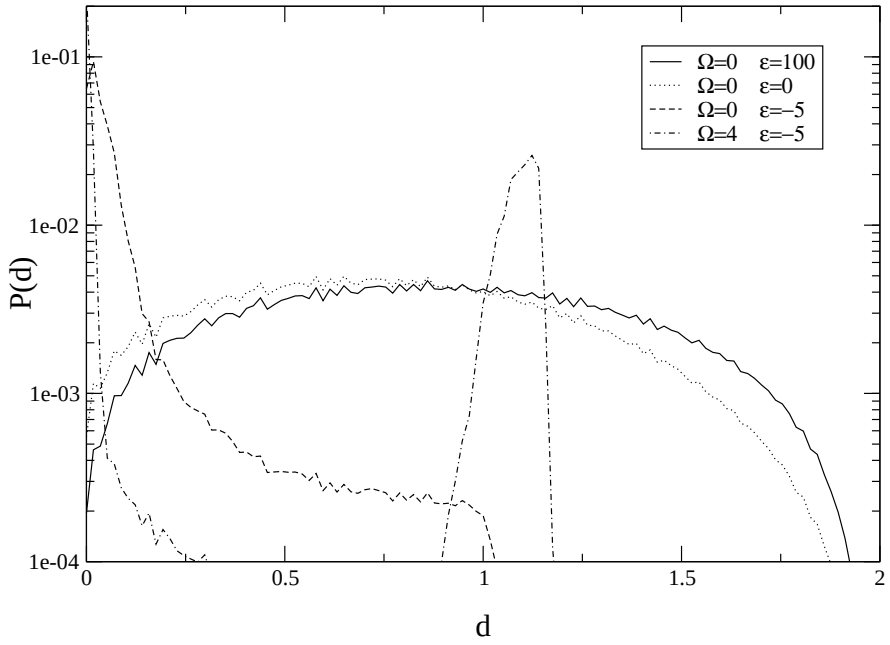

Figure 6.6: Distance distribution $P(d)$ for different values of (ϵ, Ω). At high energy $P(d)$ corresponds to a random distribution (see Fig. 6.5 on the facing page). For $\Omega = 0$ and at low energy, $P(d)$ has one peak at $d \approx 0$; almost all particles are very close from each other, and there is a single cluster collapse phase. For $\Omega \neq 0$ there are two peaks at low energy: one at very small d which is a sign of clusterisation and another peak at large d which signals multiple clusterisations; in fact there are two clusters (see text).

(c) For the ring case a trace of the two peaks still exists but they are not well separated because a lot of intermediate distances are compatible with this model.

(d) When the particles are uniformly distributed $P(d)$ has a binomial-like shape.

$P(d)$ has also been estimated for the present gravitational system, as shown on Fig 6.6. At high energy, $P(d)$ corresponds to the randomly distributed case (see Fig. 6.5 on the facing page). At low energy with $\Omega = 0$, $P(d)$ has only one peak at $d = 0$, this corresponds clearly to a single cluster case surrounded by some gas. For $\Omega \neq 0$ and at low energy (in Fig. 6.6 $\epsilon = -5$ and $\Omega = 4$), there are two well separated peaks, one at small $d_0 = 0$ and the other at $d_1 \simeq 1.1$. The peaks imply the presence of at least two clusters. However, the fact that the widths of the peaks are small excludes a large number of clusters and even more the ring case (see Fig. 6.5). Now one can combine this information with the one obtained from the study of the radial density $\rho(r)$ (see Fig. 6.4 on page 97). For $\epsilon = -5$ and $\Omega = 4$, ρ has two peaks at $r_1 \simeq 0.15$ and $r_2 \simeq 1$. All in all, this means that there are, in the mean, two clusters rotating around the center of mass. The distance between these clusters is $r_1 + r_2 \simeq 1.15 \simeq d_1$. Their mass ratio is $\frac{m_2}{m_1} = \frac{r_1}{r_2} \simeq 0.15$. Since the total mass is $m_1 + m_2 = 20$, hence $m_1 \simeq 17$ and $m_2 \simeq 3$.

The distance distribution can be of great help to identify the mass distributions at low energies. However at the transition regions since there is a superposition of different types of mass distributions the knowledge ρ and $P(d)$ is not sufficient and therefore of no help if one wants to study for example the "fractality" of the mass distribution as it has been

done in other self–gravitating systems [DVS00, SIM$^+$00], and further work is needed to get a more detailed picture.

At very low energy, near the ground state at least one of the clusters (the smallest) is very close to the boundary. There the assumption of a small evaporation rate made in chap. 5 on page 87 does not hold.

6.4.3 Phase diagram

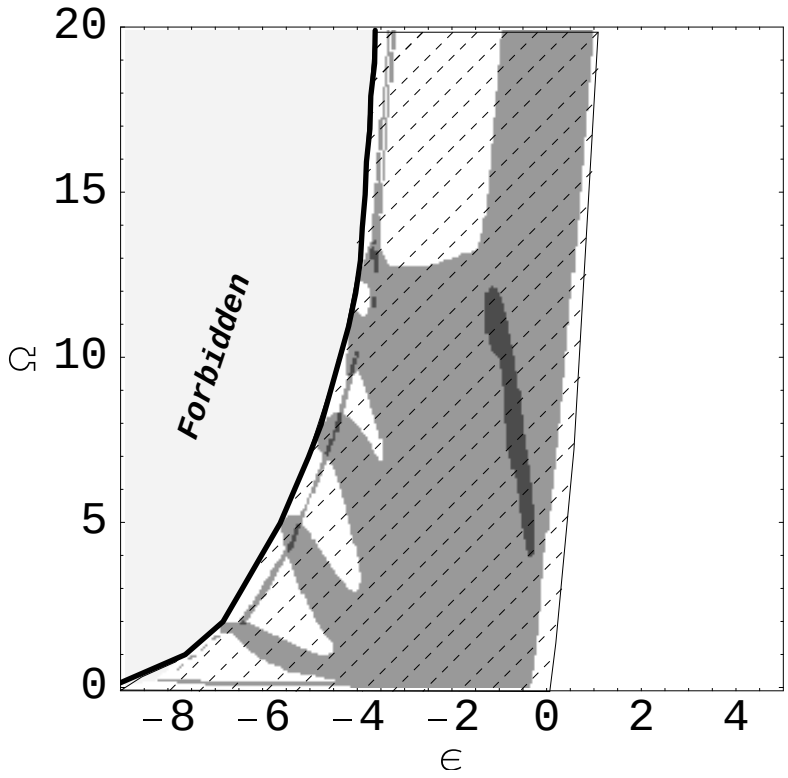

Figure 6.7: Sign of the largest eigenvalues of H_S the Hessian matrix of S as defined in chapter 2. The white regions correspond to $\lambda_1 < 0$. These are pure phase regions. The gray region corresponds to $\lambda_1 > 0$ and $\lambda_2 < 0$ and the dark gray ones also to $\lambda_1 > 0$ but $\lambda_2 > 0$. λ_2 is the second eigenvalue of H_S. $\lambda_1 > 0$ defines first order phase transition regions (see text). Points in G (the region filled with dashed lines) correspond to *local* maxima (minima) of $f(X, X_0) = -x_0 \cdot X + S(X)$ (see eq. (1.12) on page 7) if $\lambda_1(X_0) < 0$ ($\lambda_1(X_0) > 0$). Points outside G correspond to *global* maxima of $f(X, X_0)$. There is a one–to–one mapping between the microcanonical ensemble and the GBE only outside the G region (see text). S is not defined in the *forbidden* region, here in light gray. Note that (a) the points at $\Omega = 0$ and low energies $\epsilon < -7$ are not included in G, (b) the high energy limit of G is known only approximatively.

In Fig. 6.7, the sign of λ_1 as a function of ϵ and Ω is plotted. λ_1 is the largest eigenvalue of the Hessian matrix of S (see sec. 1.2.2 on page 8)

$$H_s = \left\| \begin{array}{cc} \frac{\partial^2 S}{\partial \epsilon^2} & \frac{\partial^2 S}{\partial \epsilon \partial l} \\ \frac{\partial^2 S}{\partial l \partial \epsilon} & \frac{\partial^2 S}{\partial l^2} \end{array} \right\|. \tag{6.25}$$

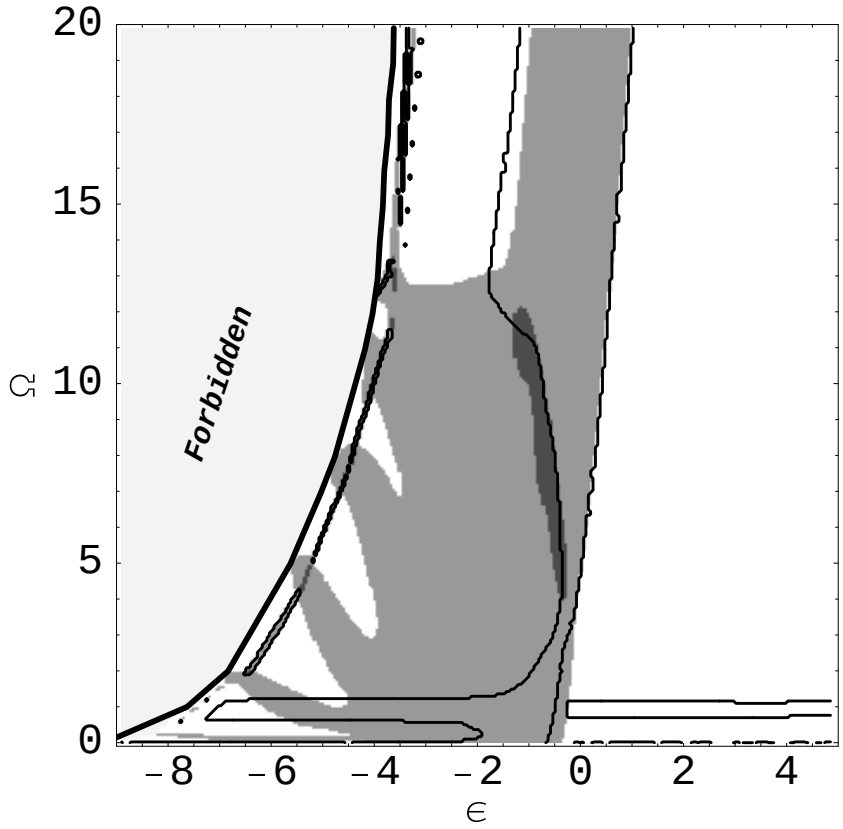

Figure 6.8: Locus of second order phase transitions (see text).

This plot can be taken as the phase diagram of the self–gravitating system at fixed ϵ *and* l. The white regions correspond to pure phases ($\lambda_1 < 0$). At high energy there is a homogeneous gas phase and at low energy there are several pure collapse phases with one ($l = \sqrt{\Omega} = 0$) or two ($l \neq 0$) clusters. The different 2–clusters phases are characterized by the relative size of their clusters (see sec. 6.4.2). These regions are separated by first order phase transition regions where $\lambda_1 > 0$ (gray in Fig. 6.7). There is even one region (dark gray) where the entropy S is a *convex* function of ϵ and l; i.e. all the eigenvalues of H_S are positive ($\lambda_1 > 0$ *and* $\lambda_2 > 0$). This region is rather stable with respect to the number of particles (at least for $N \lesssim 100$). Its specific surface slightly increases with the number of particles N.

The orientation of $\mathbf{v}_1$ the eigenvector associated with λ_1 (defined as the largest eigenvalue of H_S) is not yet known in details for all (ϵ, l). However it can already be stated that at "high" energy $\mathbf{v}_1$ is almost parallel to the energy axe (phase transition in the ϵ direction) and should be parallel to the ground state at very low energy. The overall structure of the collapse phases matches the one of the angular velocity ω (see Fig. 6.3 on page 96): roughly, the peaks in ω correspond to pure phases while the valleys between these peaks belong to the first order phase transition region.

As already mentioned, unlike in the model presented by Laliena in [Lal99] there is no critical angular momentum L_c above which the first order phase transition vanishes giving rise to a second order phase transition at L_c. Nevertheless this does not exclude second order phase transition (critical point) at all. They are defined in the microcanonical

ensemble by: (i) $\lambda_1 = 0$; (ii) $\nabla\lambda_1 \cdot \mathbf{v}_1 = 0$ (see sec. 2.3 on page 30). On Fig. 6.8 on the page before (just like on Fig. 6.7 on page 100) regions where $\lambda_1 < 0$ (> 0) are in white (gray). The condition (i) is simply achieved at the boarder between the gray and the white regions. The thick lines on Fig. 6.8 correspond to condition (ii). Second order phase transitions are located at the crossing points points of the thick lines and the boarders. One immediately sees that there are several critical points. However there are not all of (astro–)physical interest since most of them are close to the ground states line or at very high angular momentum where the small evaporation rate assumption is not valid. Nevertheless there are two points one at $(\epsilon, \Omega) \approx (-0.5, 1)$ and another one at $(\epsilon, \Omega) \approx (0, 4)$ where this assumption is valid and therefore they deserve further investigations and especially regarding their corresponding mass distributions.

6.4.4 Loss of information in CE

In a recent paper Klinko and Miller have studied another model for rotating self–gravitating systems [KM00]. They introduced the canonical analogous of the $X = \{\epsilon, \Omega = l^2\}$ ensemble namely the $x = \{\beta, \gamma\}$ ensemble (GBE), see eq. (6.6) and (6.9) on page 90.

If one inspects the entropy surface $S(X)$ (see Fig. 6.1 on page 94) it is clear that conditions (1') [e] or (2') [f] are not satisfied for all the points in the region filled with dashed lines (G) in Fig. 6.7 on page 100. This is due to the concavity of the energy ground state $\epsilon_g(\Omega)$. G includes all the two–clusters collapsed phases, the first and second order phase transitions (except for $\omega = \gamma = l = 0$). All the information contained in G is smeared out through the Laplace transform linking ME and GBE (eq. (1.12) on page 7) and, in practice, lost.

The fact that GBE misses all the two–clusters collapse phases would already be enough to disqualify it as being a good approximation (mathematical trick) of the ME. But, furthermore, if one studies more carefully $f(X, X_0) = f(X, x_0 = \frac{\partial S}{\partial X}|_{X_0}) = -x_0 \cdot X + S(X)$, $X_0 \in G$; one will notice that (a) there is one local maximum at $\Omega = 0$ and (b) there is no maximum for high Ω: in the direction of increasing Ω at low energy, $f(X, x_0)$ is a never ending increasing function, i.e. $f(X, x_0)$ has *no global maximum* for $X \in G$ (see Fig. 6.9 on the next page). Therefore the integral in eq. (1.12) on page 7 *diverges* for all x_0, $X_0 \in G$. In other words the GBE, for the present model, is *not defined* for high β and $\gamma \neq 0$ ($\omega \neq 0$). Although this result can sound very surprise, it is a direct consequence of the quasi–linear behavior of the ground state of S as a function of $\Omega \sim L^2$, hence a similar result can be found for the van der Waals gas presented in chapter 1. The domain of definition of the entropy of this model ($\neq$ domain of physical validity) is convex, and there is a region where although the conjugates of the entropy are clearly defined in the microcanonical ensemble [g], the partition sum *diverges* for these values of the intensive parameters.

One could argue that GBE is not the correct canonical ensemble (CE) for this system. I.e. one should rather fix the conjugate of ϵ and l, the inverse temperature β and the angular velocity ω, respectively.

In order to simplify the discussion, the microcanonical entropy S is plotted in fig. 6.10 (see also fig. 6.1 on page 94) as a function of the energy and the angular momentum l.

[e] $\langle X \rangle_{\mathrm{CE}} = X_0$, see sec. 1.2.3 on page 10.

[f] Small fluctuations of X in GBE, see sec. 1.2.3 on page 10.

[g] The conjugates are clearly defined from a mathematical point of view, physically it is not the case since there the pressure is *negative*.

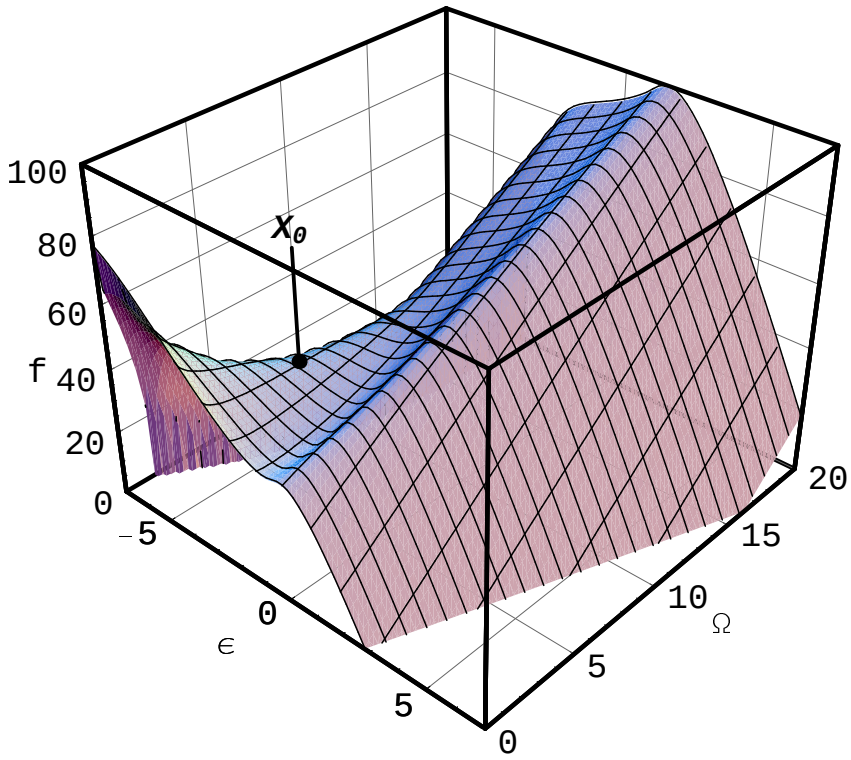

Figure 6.9: $f(\epsilon, \Omega, \beta_0, \gamma_0) = -\epsilon\beta_0 - \Omega\beta_0\gamma_0 + S(\epsilon, \Omega) - K$ as a function of ϵ and Ω, where K is an arbitrary constant; $\beta_0 = \beta(\epsilon_0, \Omega_0)$; $\Omega_0 = \Omega(\epsilon_0, \Omega_0)$; $X_0 = (\epsilon_0, \Omega_0) = (-3, 5) \Rightarrow (\Omega_0, \gamma_0) \approx (27.9, -0.196)$. The mesh lines are at constant ϵ or constant Ω. As expected f has a saddle point at $X_0 \approx (\beta_0, \gamma_0)$ since $\lambda_1(X_0) > 0$ and $\lambda_2(X_0) < 0$ (see text and Fig. 6.7 on page 100). f has a global maximum at $\Omega = 0$ and $\epsilon \approx -7$, but one sees that it is an monotonically increasing function for increasing Ω and $\epsilon(\Omega) \approx \epsilon_g(\Omega) + 2$. Therefore the integral in eq. (1.12) on page 7 *diverges* and the $(\beta, \gamma\beta)$ ensemble is *not defined* for (β_0, γ_0).

One can clearly distingish two parts. One for $0 \leq l \lesssim 4$ and the other with $l \gtrsim 4$. The ground states at $l < 4$ correspond to the two asymetric clusters cases (except at $l = 0$) whereas for $l > 4$ two equal size clusters compose the ground states. At large l, the ground states line is convex as a function of l, i.e. $\frac{\partial^2 \epsilon_g}{\partial l^2} > 0$. Hence, the origin of the divergences in GBE is removed in CE. However, one can directly conclude from fig. 6.10 that no point $X_0 = (\epsilon_0, l_0)$ in the region where $\epsilon \lesssim 0$ and $l \lesssim 5$ corresponds to a global maximum of the function $f(\epsilon, l, \beta_0, \omega_0) = -\epsilon\beta_0 - l\beta_0\omega_0 + S(\epsilon, l)$ (for an example see fig. 6.11). This implies that all the asymetric pure phases are overlooked by CE. It can be shown that this is also the case for the two critical regions at relatively high energies.

All the examples of this section show how dramatic can be the information loss if one studies an isolated system in ensembles where the intensive variables are fixed.

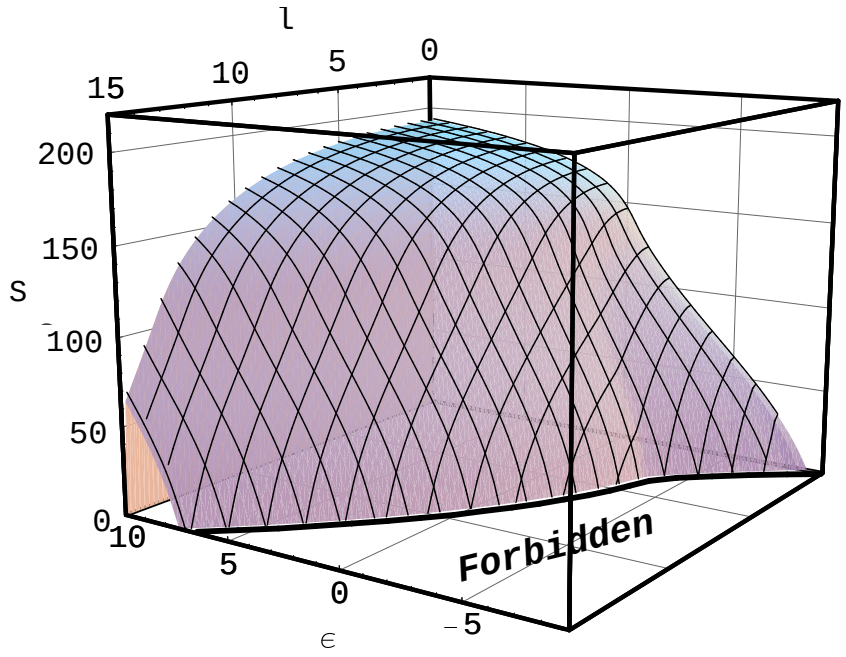

Figure 6.10: Entropy surface as function of $l = \sqrt{\Omega}$ and ϵ. The mesh line are at constant l or ϵ. The thick line is the projection of the ground states. S is not defined in the *forbidden* region.

6.5 Discussion and conclusions

In this chapter the results of the study of the equilibrium properties of a self–gravitating system is presented. The "extensive" dynamical quantities are the total energy E and the angular momentum L. This is the first study where no assumption is made about the spatial properties of the mass distribution.

It is shown that the conservation of the angular momentum plays a non-trivial role. One can find that these systems have a surprisingly rich phase diagram with a large first order phase transition region and also non trivial second order phase transitions.

All the phase diagram is not of physical relevance since near the ground states line the small evaporation rates assumption breaks down. Nevertheless, there are two critical regions at relatively high energies which could be of astrophysical importance. Further studies are needed to

- localize more precisely these critical regions,
- check their presence for systems with large number of particles,
- study their corresponding mass distribution.

There is no heat bath for astrophysical system. But if one uses the canonical ensemble as a mathematical trick one would loose all the information about

- the asymmetric cluster phases,
- the first order transition region,

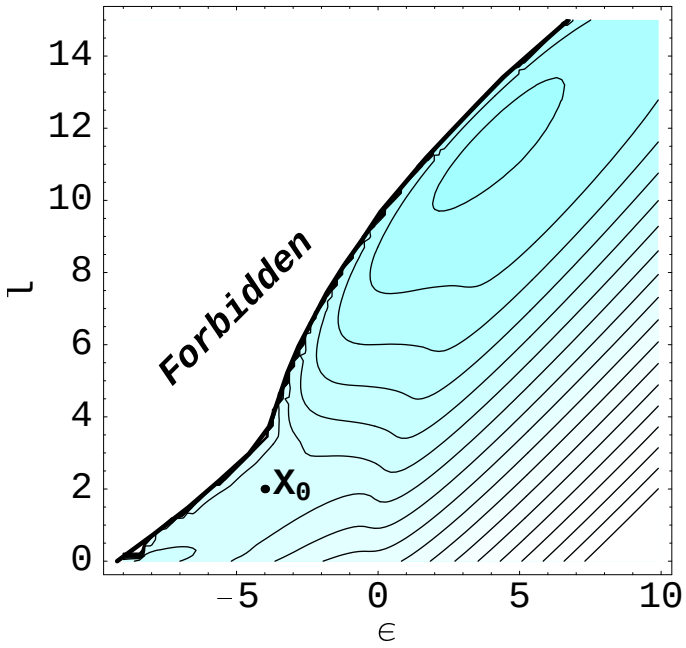

Figure 6.11: Contour-density plot of $f(\epsilon, l, \beta_0, \omega_0) = -\epsilon\beta_0 - l\beta_0\omega_0 + S(\epsilon, l) - K$ as a function of ϵ and l, where K is an arbitrary constant; $\beta_0 = \beta(\epsilon_0, l_0)$; $\omega_0 = \omega(\epsilon_0, l_0)$. $X_0 = (\epsilon_0, l_0) = (-4, 2)$. As expected f has a saddle point at $X_0 = (\beta_0, l_0)$ since $\lambda_1(X_0) > 0$ and $\lambda_2(X_0) < 0$ (see text and Fig. 6.7 on page 100). The main contribution to the partition sum for these values of the intensive variables comes from points located toward $(\epsilon, l) \approx (5, 12)$. Hence, in CE at (β_0, ω_0), The mass distribution is composed by two equal-size clusters rotating with large mean energies and angular momentum. This is in sharp constrast to the physical situations at X_0. f is not defined in the *forbidden* region.

- the critical point.

Furthermore, for a particular choice of intensive variables the partition sum *diverges* for some (microcanonically defined) values of these intensives variables.

Of course, it just an *equilibirum statistical* model that is presented. It may help to understand the physics of globular clusters or collapsing molecular clouds, but the results should be interpreted with caution especially in the case of star formation. A lot of "ingredients" are missing in order to have a complete picture of the formation of multiple stars systems and planetary systems, for instance the magnetic field [HMCB00, GSLL00], or the presence of vortices [CHA00].

The study of such self-gravitating system is in its infancy [LL96A, LAL99]. There are a lot of research directions.

The main weakness of the results presented in this chapter is the very limited number of particles that could be considered. Though, in many cases, in astrophysical context all the qualitative equilibrium behaviors could be given with small number of particles (see e.g. Padmanabhan and its two particles models in [PAD90]). However, if one wants to study the equilibrium properties of galaxies, one cannot be completely satisfied with results obtained from 20 particles models. Work is in progress to increase the number of particles and also to study the system in 3-dimensional space.